

Resolving Hubble Tension by Self-Interacting Neutrinos with Dirac Seesaw

HONG-JIAN HE,^{a,b,c*} YIN-ZHE MA,^{d,e†} JIAMING ZHENG^{a‡}

^a Tsung-Dao Lee Institute & School of Physics and Astronomy,
Shanghai Jiao Tong University, Shanghai 200240, China

^b Institute of Modern Physics and Department of Physics,
Tsinghua University, Beijing 100084, China

^c Center for High Energy Physics, Peking University, Beijing 100871, China

^d School of Chemistry and Physics, University of KwaZulu-Natal,
Westville Campus, Private Bag X54001, Durban, 4000, South Africa

^e NAOC-UKZN Computational Astrophysics Centre (NUCAC),
University of KwaZulu-Natal, Durban, 4000, South Africa

Abstract

Self-interacting neutrinos that begin to free-stream at close to matter-radiation equality can reduce the physical size of photon sound horizon at last scattering surface. This can be the reason why standard Λ CDM cosmology sees a lower value of Hubble constant than local measurements from distance ladder. We propose a new realization of self-interacting Dirac neutrinos (SID ν) with light dark photon mediator for a viable interaction mechanism. Our model is UV completed by a Dirac seesaw with anomaly-free dark $U(1)_X$ gauge group which charges the right-handed neutrinos. This naturally generates small masses for Dirac neutrinos and induces self-scattering of right-handed neutrinos. The scattering with left-handed neutrinos is suppressed by a chirality-flip mass insertion when the neutrino energy is much larger than its mass. The resultant neutrino self-scattering is not operative for $E_\nu \gtrsim O(\text{keV})$, which avoids the cosmological and laboratory constraints. By evolving Boltzmann equations for left- and right-handed neutrino number densities, we show that about 2/3 of the left-handed neutrinos are converted into right-handed neutrinos in a short epoch between the Big-Bang Nucleosynthesis and the recombination, and interact with each other efficiently afterwards. The resultant neutrino non-free-streaming is the key ingredient to shrink down the comoving sound horizon at drag epoch, which can reconcile the Hubble tension between early and late time measurements.

[e-Print: arXiv:2003.12057]

*Email: hjhe@sjtu.edu.cn

†Email: ma@ukzn.ac.za

‡Email: zhengjm3@sjtu.edu.cn

Contents

1. Introduction	2
2. Interacting Dirac Neutrinos from Dirac Seesaw.....	4
3. Cosmological Evolution of Interacting Right-Handed Neutrinos	7
4. Evolution of Neutrino Densities by Numerical Analysis	12
5. Conclusions.....	16
A.Neutrino Chirality Flip via Mass-Insertion	18
B.Boltzmann Equations and Cross Sections	18
References	21

1. Introduction

The discrepancy between measurements of the Hubble constant H_0 from the observations of the early Universe and from the late time observations poses a serious challenge to the conventional Λ -Cold Dark Matter (Λ CDM) cosmology [1, 2]. In particular, *Planck* space telescope measures H_0 from the cosmic microwave background (CMB) and gives $H_0 = 67.4 \pm 0.5 \text{ km s}^{-1} \text{ Mpc}^{-1}$ [3], with a precision better than 1%. This is compatible with the independent result from Baryon Acoustic Oscillation (BAO) & Dark Energy Survey (DES) & Big Bang Nucleosynthesis data [4], which gives $H_0 = 67.4^{+1.1}_{-1.2} \text{ km s}^{-1} \text{ Mpc}^{-1}$. In contrast, the distance ladder measurement (SH0ES) by using Type-Ia supernovae calibrated by Cepheid favors a larger Hubble constant, $H_0 = 74.0 \pm 1.4 \text{ km s}^{-1} \text{ Mpc}^{-1}$ [5]. Although the systematic uncertainty of the distance ladder measurement is under debate [6], its value is consistent with another completely independent measurement of the strong lensing time-delay effect. By measuring six distant quasar time-delays, the H0LiCOW team determines $H_0 = 73.3^{+1.7}_{-1.8} \text{ km s}^{-1} \text{ Mpc}^{-1}$ [7]. This solidifies the the discrepancy between high-redshift measurements and local measurements. The recent survey on various H_0 measurements concludes that the H_0 discrepancy between early and late Universe observations ranges from 4σ to 6σ , and is robust to the exclusion of any one method, team or source [2].

A physically attractive resolution to the Hubble tension is the scenario of self-interacting neutrinos [8, 9, 10, 11, 12, 13], but its viable realization was found to be highly challenging [12]. In this scenario, the onset of neutrino free-streaming is delayed in the early uni-

verse and the resultant phase shift and amplification of acoustic peaks in the CMB power spectrum can be compensated by shifts of other cosmological parameters [8, 9, 14, 15]. In particular, Refs. [9, 12] found that if the active neutrinos self-interact through an effective vertex

$$\mathcal{L}_{\text{eff}} = G_{\text{eff}} \bar{\nu} \nu \bar{\nu} \nu, \quad (1.1)$$

a larger Hubble constant $H_0 = 72.3 \pm 1.4 \text{ km s}^{-1} \text{ Mpc}^{-1}$ (with $\Delta N_{\text{eff}} \approx 1$) can be accommodated by the CMB observation for the “strongly interacting” regime and “moderately interacting” regime with $\log_{10}(G_{\text{eff}} \text{MeV}^2) = -1.35_{-0.066}^{+0.12}$ and $-3.90_{-0.93}^{+1.0}$, respectively. Ref. [9] considered an effective interaction of neutrino mass-eigenstates in the form

$$\mathcal{L} = g_{ij} \bar{\nu}_i \nu_j \varphi, \quad (1.2)$$

and found that the Hubble tension can be evaded with $G_{\text{eff}} \equiv g^2/m_\varphi^2 = (10^{-1} - 10^{-4}) \text{ MeV}^{-2}$ and $\Delta N_{\text{eff}} \approx 1$. However, Ref. [10] found that neutrino self-interactions induced by a very light or massless mediator cannot resolve the Hubble tension. Ref. [11] considered a possibility that the neutrino free-streaming is impeded by the “dark neutrino interaction” between neutrinos and the dark matter, and found that the phase shift of non-free-streaming neutrinos alone can raise the CMB determined Hubble constant to $H_0 = 69.39_{-0.68}^{+0.69} \text{ km s}^{-1} \text{ Mpc}^{-1}$ without additional ΔN_{eff} . These suggest that the Hubble tension could be resolved if the neutrino free-streaming does not turn on before $T \sim 10 \text{ eV}$ when the modes relevant to the observed CMB power spectrum enter the horizon. But the neutrino self-interactions (1.1) and (1.2) are *not gauge-invariant*. It was found that a UV completion is highly constrained and almost excluded by cosmological observations such as the Big Bang Nucleosynthesis (BBN) [12, 16, 17, 18], or by laboratory bounds such as meson decays [12, 19, 20, 21]. Furthermore, the light neutrinos have to be Majorana type, the neutrino self-interaction needs to be flavor-dependent, and the UV-completion model requires a nonminimal mechanism to simultaneously generate neutrino masses and appreciable self-interactions [12]. Some other different attempts to alleviate the Hubble tension with neutrino physics appeared in [22, 23, 24, 25].

In this work, we propose a physically attractive model of self-interacting Dirac neutrinos (SID ν) with light dark photon mediator to delay the neutrino free-streaming time-scale, and thus shrink the comoving sound horizon at the last scattering surface (r_*) without drastically affecting the projected Silk damping scale (ℓ_d). Such modification of the early time physics will result in an increased Hubble rate inferred by the CMB measurement. Our new model is UV-completed by a Dirac seesaw with an anomaly-free dark $U(1)_X$ gauge group which charges the right-handed neutrinos and is spontaneously broken. This naturally generates small masses for Dirac neutrinos and simultaneously induces self-interacting scattering of right-handed neutrinos. Thus, different from what

was done in the literature [9, 10, 11, 12], our model has the right-handed neutrinos (rather than the left-handed ones) interact with the dark photon X^μ (rather than a scalar φ) at an energy scale of $O(\text{MeV})$. The dark photon X^μ serves as the mediator of the hidden neutrino interaction, which is a key ingredient of our scenario. In the early Universe, only left-handed neutrinos are abundantly produced from the thermal bath of the standard model (SM) particles by electroweak interactions. The scattering amplitude of neutrinos through the dark photon exchange is suppressed by a chirality-flip (mass-insertion) factor m_ν/E_ν for each left-handed neutrino participating in the scattering, where E_ν and m_ν are the neutrino energy and mass, respectively. Hence, the production of right-handed neutrinos and the mediator particles from left-handed neutrino scattering is suppressed at high temperature, so it is free from cosmological constraints such as the strong BBN bound. As the temperature decreases, the chirality-flip factor becomes larger and has less suppression. At the temperature $T_c \ll O(\text{MeV})$, the small amount of right-handed neutrinos produced out-of-equilibrium start to scatter effectively with left-handed neutrinos, and trigger a rapid conversion of left-handed neutrinos to the right handed ones. Eventually, the cosmic neutrino relics are composed of both left-handed and right-handed neutrinos which scatter efficiently with each other until the decoupling of the dark photon interaction at which the neutrinos begin to free-stream. In this way, we build up a consistent and novel realization of the self-interacting neutrino scenario as a resolution to the Hubble tension, which overcomes all the difficulties in the previous proposal [9]. Moreover, our model naturally generates the small Dirac neutrino masses and does not require any special flavor structure of the neutrino interaction to evade all the existing cosmological and laboratory constraints [12].

The rest of this paper is organized as follows. In Section 2, we propose a new realization of Dirac neutrino seesaw as the UV completion of self-interacting neutrinos in the early Universe. In Section 3, we analyze qualitatively the evolution of the right-handed neutrinos in the early Universe and the condition to delay the free-streaming, while evading the cosmological and laboratory constraints. In Section 4, we perform a numerical analysis to evolve the neutrino number density by Boltzmann equations as an explicit demonstration of the physical picture described in Section 3. Finally, we conclude in Section 5. We present the technical details in Appendices A and B.

2. Interacting Dirac Neutrinos from Dirac Seesaw

In this section, we show that the neutrino self-interaction can be naturally realized in a new Dirac seesaw model of neutrinos with a dark $U(1)_X$ gauge group. The Dirac seesaw was proposed [26] to generate small Dirac masses for light neutrinos. Its key part contains the right-handed neutrinos with charge $-1/2$ under a hidden dark $U(1)_X$

Groups	L_j	H	Φ_1	Φ_2	S	R_{1j}	R_{2j}
$SU(2)_L$	2	2	2	2	1	1	1
$U(1)_Y$	$-\frac{1}{2}$	$-\frac{1}{2}$	$-\frac{1}{2}$	$-\frac{1}{2}$	0	0	0
$U(1)_X$	0	0	$\frac{1}{2}$	$-\frac{1}{2}$	$\frac{1}{2}$	$-\frac{1}{2}$	$\frac{1}{2}$

Table 1: Assignments for the Dirac seesaw model under the extended electroweak gauge group $SU(2)_L \otimes U(1)_Y \otimes U(1)_X$. Here $j (= 1, 2, 3)$ denotes the index of fermion families.

gauge group. This $U(1)_X$ is spontaneously broken by a weak singlet scalar S at the TeV scale (or somewhat below) which has a $U(1)_X$ charge 1/2. This can generate a gauge-invariant dimension-5 effective operator at the weak scale for the Dirac neutrino mass generation, $\mathcal{O}_5 = \frac{1}{\Lambda} \bar{L} H S \nu_R$, where Λ is a high energy cutoff scale, L the left-handed lepton doublet and H the SM Higgs doublet. So the light neutrinos acquire small Dirac masses $m_\nu \sim \langle H \rangle \langle S \rangle / \Lambda$.

For this study, we propose a new realization of the Dirac seesaw mechanism with an anomaly-free dark $U(1)_X$ gauge group and an exact \mathbb{Z}_2 symmetry. This naturally extends the previous simple model [26] which was not UV-completed for anomaly cancellation. We present this model in Table 1, where Φ_1 and Φ_2 are two new heavy Higgs doublets with mass $M_\Phi = O(10^9 \text{ GeV})$. The light singlet scalar S acquires a vacuum expectation value (VEV) of $O(\text{MeV})$ and spontaneously breaks $U(1)_X$ gauge group, leading to a dark photon of mass around $O(\text{keV})$. R_{1j} and R_{2j} are two right-handed Dirac fermions which carry opposite $U(1)_X$ charges to cancel the gauge anomaly, where $j (= 1, 2, 3)$ denotes the fermion family index. As we will show shortly, the combination $R_{1j} + R_{2j}$ just gives the right-handed neutrinos ν_{Rj} . Thus, we can write down the Lagrangian terms relevant to the Dirac seesaw,

$$\begin{aligned} \Delta \mathcal{L} \supset & -y_{ij} \bar{L}_i (\Phi_1 R_{1j} + \Phi_2 R_{2j}) + M_3 (S \Phi_1^\dagger + S^* \Phi_2^\dagger) H + \text{h.c.} \\ & -M_\Phi^2 (|\Phi_1|^2 + |\Phi_2|^2), \end{aligned} \quad (2.1)$$

where $i, j = 1, 2, 3$ are the family indices, and the trilinear scalar coupling may be around the Φ mass scale, $M_3 = O(M_\Phi)$. The Lagrangian is invariant under the following \mathbb{Z}_2 symmetry,

$$\mathbb{Z}_2: \quad B^\mu \leftrightarrow B^\mu, \quad X^\mu \leftrightarrow -X^\mu, \quad \Phi_1 \leftrightarrow \Phi_2, \quad S \leftrightarrow S^*, \quad R_{1j} \leftrightarrow R_{2j}, \quad (2.2)$$

where B^μ and X^μ are gauge bosons of $U(1)_Y$ and $U(1)_X$, respectively. The above \mathbb{Z}_2 assignments can be re-expressed as follows,

$$\begin{aligned} \text{Fields :} & \quad B^\mu & X^\mu & \Phi_1 \pm \Phi_2 & S \pm S^* & R_{1j} \pm R_{2j} \\ \mathbb{Z}_2 : & \quad + & - & \pm & \pm & \pm \end{aligned} \quad (2.3)$$

This \mathbb{Z}_2 symmetry forbids the kinetic mixing between X^μ and B^μ to all loop orders, and thus can evade possible astrophysical constraints on the light dark photons [28]. Since $M_\Phi \gg m_S, m_H$, we can integrate out the heavy fields Φ_1 and Φ_2 by using their equations of motions,

$$\Phi_1 = \frac{M_3}{M_\Phi^2} HS - \frac{y_{ij}^*}{M_\Phi^2} \bar{R}_{1j} L_i + \dots, \quad (2.4a)$$

$$\Phi_2 = \frac{M_3}{M_\Phi^2} HS^* - \frac{y_{ij}^*}{M_\Phi^2} \bar{R}_{2j} L_i + \dots. \quad (2.4b)$$

With this we can deduce the following effective Lagrangian from Eq.(2.1),

$$\Delta\mathcal{L} = -\frac{y_{ij} M_3}{M_\Phi^2} \bar{L}_i H (S R_{1j} + S^* R_{2j}) + \text{h.c.} + \dots \quad (2.5)$$

Integrating out the heavy Higgs doublets $\Phi_{1,2}$ will also induce a correction to the quartic coupling $\sim (M_3^2/M_\Phi^2)|S|^2|H|^2$, which is added to the original tree-level Higgs portal term $|S|^2|H|^2$ with a total coupling λ_{SH} . For the current setup, we set the coupling $\lambda_{SH} = 0$ at tree level. This choice is technically natural since the $|S|^2|H|^2$ vertex will remain vanishing at loop levels. We note that including the graviton-exchange contribution between S and H could only induce a nonlocal interaction between $|S|^2$ and $|H|^2$, which is also fully negligible for the current study. With $\lambda_{SH} = 0$, we can maintain a light scalar S with $m_S \ll M_h$ where $M_h \simeq 125$ GeV is the SM Higgs boson mass, while at the same time this avoids the production of S through the Higgs portal coupling in the early Universe.

After S and H develop the VEVs $\langle S \rangle = v_s/\sqrt{2}$ and $\langle H \rangle = (v_h/\sqrt{2}, 0)$, we find that the neutrinos acquire the following Dirac mass term,

$$\begin{aligned} \mathcal{L}_\nu &= -m_{\nu ij} \bar{\nu}_{L_i} \nu_{R_j} + \text{h.c.}, \\ m_{\nu ij} &= y_{ij} \frac{v_s v_h M_3}{\sqrt{2} M_\Phi^2}, \end{aligned} \quad (2.6)$$

where the right-handed neutrinos ν_{R_j} are defined by the following rotation,

$$\begin{aligned} \nu_{R_j} &= \frac{1}{\sqrt{2}} (R_{1j} + R_{2j}), \\ \nu_{s_j} &= \frac{1}{\sqrt{2}} (R_{1j} - R_{2j}), \end{aligned} \quad (2.7)$$

which holds for each given flavor index j . The orthogonal state ν_{s_j} is \mathbb{Z}_2 odd. It has no left-handed partner and will remain massless. Eq.(2.6) realizes the Dirac seesaw and can generate naturally small neutrino masses. For instance, setting $y_{ij} = O(1)$, $M_3 = O(M_\Phi) = O(10^9)$ GeV, and $v_s = O(\text{MeV})$, we obtain $m_{\nu ij} = O(0.1)$ eV, which agrees with the current neutrino oscillation data [27].

Since the SM Higgs boson mass M_h is much larger than the masses of the light scalar S and gauge boson X^μ as well as the Dirac neutrinos (ν_L, ν_R), it is more convenient to

integrate out the SM Higgs doublet H in the low energy effective theory of S , X^μ and $\nu_{L,R}$. The neutrino effective interactions then take the following form,

$$\mathcal{L} = -y'_{ij}\bar{\nu}_{Li}\nu_{Rj}S + \frac{g_x}{2}\bar{\nu}_{sj}\gamma^\mu\nu_{Rj}X_\mu + \text{h.c.}, \quad (2.8)$$

where the effective Yukawa coupling

$$y'_{ij} = \frac{\sqrt{2}m_{\nu ij}}{v_s}, \quad (2.9)$$

and g_x is the gauge coupling of $U(1)_X$. Setting the gauge coupling $g_x = O(0.1)$ and the scalar VEV $v_s = O(\text{MeV})$, we find that the dark photon X^μ acquires a small mass via spontaneous symmetry breaking, $m_X = g_x v_s = O(\text{keV})$.

We will demonstrate that the $U(1)_X$ gauge coupling can generate the desired neutrino self-interaction with scale $\langle S \rangle = O(\text{MeV})$ to resolve the Hubble tension. As to be shown in the next section, the left-handed neutrino ν_L will be converted to ν_R and ν_s after the BBN, and the dark photon X^μ can mediate effective scattering among $\nu_{L,R}$ and ν_s before recombination. The resolution of Hubble tension then requires $v_s = O(\text{MeV})$ and we choose $M_\Phi = O(M_3) = O(10^9 \text{GeV})$ to generate realistic Dirac neutrino masses $m_\nu = O(0.1 \text{eV})$. With these inputs, the effective Yukawa coupling (2.9) has the size $y' = \sqrt{2}m_\nu/v_s = O(10^{-7})$.

In summary, our low energy effective theory contains the SM particle content plus additional new particles, including three light Dirac neutrinos with their right-handed component ν_{Rj} , the three right-handed massless fermions ν_{sj} , a massive dark photon X^μ which mediates the neutrino self-interaction, and a scalar Higgs boson of σ from the real component of the scalar singlet $S = \frac{1}{\sqrt{2}}(\sigma + i\omega)$. The three light Dirac neutrinos naturally acquire tiny Dirac masses $m_\nu = O(0.1 \text{eV})$ via the Dirac seesaw mechanism. In the following analysis, we will ignore the detail of the neutrino flavor mixing for simplicity. We will also set $m_X = m_\sigma$ for our parameter space, which kinematically forbids the decay channel $\sigma \rightarrow X^\mu X^\mu$.

3. Cosmological Evolution of Interacting Right-Handed Neutrinos

In this section, we study qualitatively the evolution of neutrino densities after the decoupling of electroweak interactions. The key point is that the scattering of ν_L only produces a trace amount of ν_R and ν_s in the very early Universe because of chirality suppression. As the Universe cools down, this chirality suppression will be highly reduced. So the scattering of ν_R and ν_s with ν_L becomes efficient and rapidly converts part of ν_L into ν_R or ν_s . The neutrino relic before recombination is a mixture of ν_L , ν_R and ν_s , which can couple tightly with each other through the dark photon mediator X^μ and hence delay

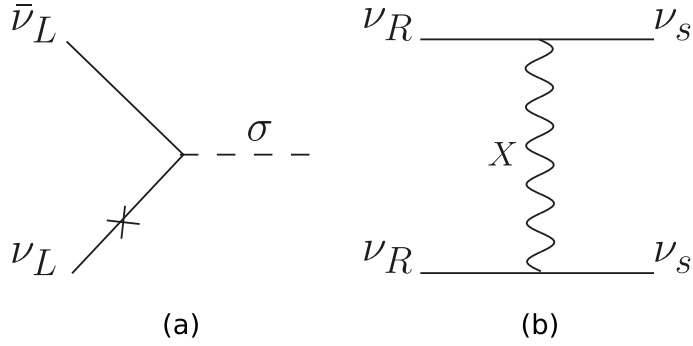


Figure 1: Panel (a): Inverse decay process $\nu_L \bar{\nu}_L \rightarrow \sigma$. The produced scalar particle σ will decay into $\bar{\nu}_L \nu_R$ and $\bar{\nu}_R \nu_L$ subsequently, and increase the ν_R density in the early Universe. Panel (b): The conversion process $\nu_R \rightarrow \nu_s$ as mediated by the dark photon X^μ .

the neutrino free-streaming time close to matter-radiation equality. We will discuss the condition for the evolution and various phenomenological constraints in this section.

Since we only consider the epoch with temperature $T \gg m_\nu$, the neutrinos are highly relativistic. So for the left-handed neutrino scattering, we can include the neutrino mass effect up to its first order via mass-insertion on each incoming state ν_L of the Feynman diagram. This induces a chirality-flip suppression factor m_ν/\sqrt{s} in the scattering amplitude. A derivation of this factor is given in Appendix A.

In the early Universe, only left-handed neutrinos ν_L are thermalized through electroweak interaction. After electroweak and $U(1)_X$ symmetry breaking, ν_L and ν_R form massive Dirac particles and oscillate into each other. The right-handed neutrinos can then be produced out-of-equilibrium via annihilation process $\nu_L \bar{\nu}_L \rightarrow \sigma$ (including a mass insertion of $m_\nu \bar{\nu}_L \nu_R + \text{h.c.}$) as shown in Fig. 1a, with the subsequent σ decays $\sigma \rightarrow \nu_L \bar{\nu}_R, \nu_R \bar{\nu}_L$.¹ The thermally averaged cross section of this process can be estimated as

$$\langle \sigma v \rangle_{LL\sigma} \approx \left(\frac{m_\nu}{m_\sigma} \right)^2 \langle \sigma v \rangle_{LR\sigma}, \quad (3.1)$$

where $\langle \sigma v \rangle_{LR\sigma}$ is the averaged cross section of $\nu_L \bar{\nu}_R \rightarrow \sigma$ given in Eq.(B.3c). We see that $\langle \sigma v \rangle_{LL\sigma}$ is highly suppressed by $m_\nu^4/(m_\sigma^2 v_s^2)$, so this annihilation process is extremely slow and always out of thermal equilibrium in the early Universe. The produced σ bosons then decay predominantly to $\nu_L \bar{\nu}_R$ and $\nu_R \bar{\nu}_L$, leading to a net increase of ν_R ($\bar{\nu}_R$) density. The small amount of produced ν_R neutrinos can scatter effectively among themselves through the $U(1)_X$ gauge interaction. To see this, we estimate the density of ν_R as $n_{\nu_R} \sim n_{\nu_L} \Gamma_\sigma H^{-1}$, where n_{ν_L} is the total left-handed neutrino density² and Γ_σ is the

¹Note that ν_R can also be produced by $2 \rightarrow 2$ scattering such as $\nu_L \nu_L \leftrightarrow \nu_R \nu_R, \nu_s \nu_s$ by exchanging a t -channel σ or X^μ . However, as will be shown below, the small amount of ν_R or ν_s is only important well after BBN. The $2 \rightarrow 2$ scattering rate at this temperature is much smaller than the inverse decay rate by a factor of T^2/v_s^2 . So we will ignore the $2 \rightarrow 2$ production processes hereafter.

²The convention of number density n_j of a particle species j in this paper is always defined as the

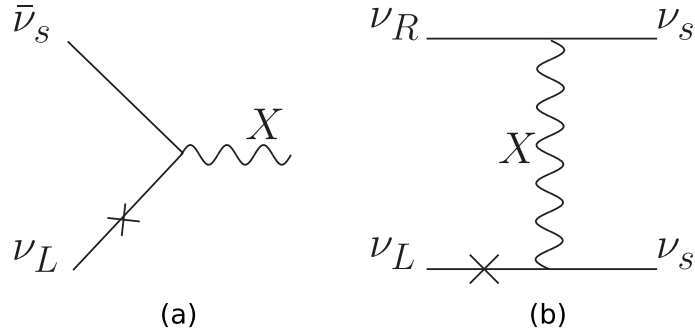


Figure 2: Conversion processes $\nu_L \rightarrow \nu_R, \nu_s$. Panel (a): The inverse decay $\nu_L \bar{\nu}_s \rightarrow X^\mu$, where the final state X^μ predominantly decays into $\nu_R \bar{\nu}_s$ or $\nu_s \bar{\nu}_R$. Panel (b): An example of the conversion process $\nu_L R \rightarrow RR$, where R denotes ν_R or ν_s (or their antiparticles) in any family.

thermally averaged decay rate of σ . The ν_R scattering process such as Fig. 1b will become efficient when

$$H \lesssim \tilde{\Gamma} \approx n_{\nu_R} \langle \sigma v \rangle_{RR} \quad (3.2)$$

with $\langle \sigma v \rangle_{RR}$ the characteristic cross section of scattering between the right-handed particles ν_R and ν_s given in Eq.(B.5a). This condition is easily satisfied during the interested epoch with $T \lesssim O(\text{MeV})$. For the similar reason, the conversion $\sigma\sigma \leftrightarrow X^\mu X^\mu$ and $\nu_R \bar{\nu}_s \leftrightarrow X^\mu$ are also efficient because they are also induced by the $U(1)_X$ interaction. Hence, a small amount of tightly coupled fluid which consists of ν_R , ν_s , σ , and X^μ is produced from ν_L scattering in the early Universe.

The generated ν_R and ν_s catalyze the conversion of left-handed neutrinos to right-handed ones through much faster conversion processes $\nu_L \bar{\nu}_s \rightarrow X^\mu$ and $\nu_L R \rightarrow RR$, as shown in Fig. 2. Here R denotes the particle from all three families of ν_R , ν_s and their antiparticles. The cross sections of both conversion processes in Fig. 2 are suppressed by one less factor of m_ν^2 than the annihilation process in Fig. 1a. The thermally averaged cross section of $\nu_L \bar{\nu}_s \rightarrow X^\mu$ and $\nu_L R \rightarrow RR$ are given by Eqs.(B.3b) and (B.5b), respectively. For $T > m_X$, the rate of the latter process is larger than the former one by a factor of T^2/m_X^2 and dominates the conversion process. As the Universe cools down, the conversion rate increases because the reaction energy is closer to the X^μ resonance and the chirality factor m_ν/E_ν also becomes larger. Below a certain temperature T_c , the $R + \nu_L$ scattering becomes efficient:

$$H \ll \Gamma_{\text{conv}} \equiv n_{\nu_L} (\langle \sigma v \rangle_{LR} + \langle \sigma v \rangle_{LRX}), \quad (\text{for } T \ll T_c). \quad (3.3)$$

The number of right-handed particles R in a conformal volume can increase exponentially in a Hubble time by a factor of $\sim e^{\Gamma_{\text{conv}}/H}$ via continuously converting ν_L to ν_R and total number density including both particles and their antiparticles from all three generations.

ν_s . This domino effect converts left-handed neutrinos to right-handed neutrinos rapidly, until $n_{\nu_L} = n_{\nu_R} = n_{\nu_s}$, a stationary configuration determined by the principle of detailed balance. The neutrinos ν_L , ν_R and ν_s scatter effectively with each other, stalling the free-streaming of neutrinos, which is the key ingredient to shrink down the r_* while keeping ℓ_d intact.

There are several conditions that needs to be satisfied by our model. The rapid conversion process should not happen before decoupling of the neutrino electroweak interaction at $T = O(\text{MeV})$. Otherwise, the right-handed neutrinos could be in equilibrium with the thermal bath and increase the total neutrino density. This can in turn populate the gauge boson X^μ of mass $m_X = O(\text{keV})$ in the early Universe, where X^μ mediates neutrino self-interaction. Such an increase of N_{eff} was severely constrained by primordial deuterium measurement and tends to disfavor the self-interacting Dirac neutrinos [12]. But we can avoid this in our model by requiring the total rate Γ_{conv} of ν_R scattering with ν_L be smaller than the Hubble rate before BBN,

$$\left. \frac{\Gamma_{\text{conv}}}{H} \right|_{\text{MeV}} \lesssim 1. \quad (3.4)$$

This imposes an upper bound on the gauge coupling g_x for each given dark photon mass m_X as shown for the case of $m_\nu = 0.05\text{eV}$ in the blue shaded region of Fig. 3. For instance, Fig. 3 gives $g_x \lesssim 2 \times 10^{-4}$ for $m_X = 10\text{eV}$, and $g_x \lesssim 25 \times 10^{-4}$ for $m_X = 10^4\text{eV}$.

Since the conversion rate peaks at $E \sim m_X$, the following condition should be satisfied as well,

$$\left. \frac{\Gamma_{\text{conv}}}{H} \right|_{T=m_X} \gtrsim 1, \quad (3.5)$$

so that the rapid conversion process $\nu_L \rightarrow \nu_R, \nu_s$ can occur in the early Universe. This excludes the yellow shaded region in Fig. 3.

The resolution of the Hubble tension requires that the neutrino non-free-streaming alters the damping tail of the CMB power spectrum [9]. The scattering should be efficient when the relevant Fourier mode corresponding to the damping tail enters the Hubble radius. As a benchmark, the Fourier modes corresponding to multipoles $\ell \sim 2000$ enter the Hubble radius at $T_t \sim 10\text{eV}$. The right-handed neutrino scattering should be efficient around this epoch and therefore satisfies

$$\left. \frac{\Gamma_R}{H} \right|_{T_t} > 1, \quad (3.6)$$

where $\Gamma_R = n_R(\langle \sigma v \rangle_{RRX} + \langle \sigma v \rangle_{RR})$ is the total rate of the $\nu_R + \nu_s$ scattering. By assuming that the left-right handed neutrino conversion already finished before this epoch, the detailed balance of the conversion processes such as $\nu_L \nu_R \leftrightarrow \nu_s \nu_s$ and $\nu_R \nu_R \leftrightarrow \nu_s \nu_s$

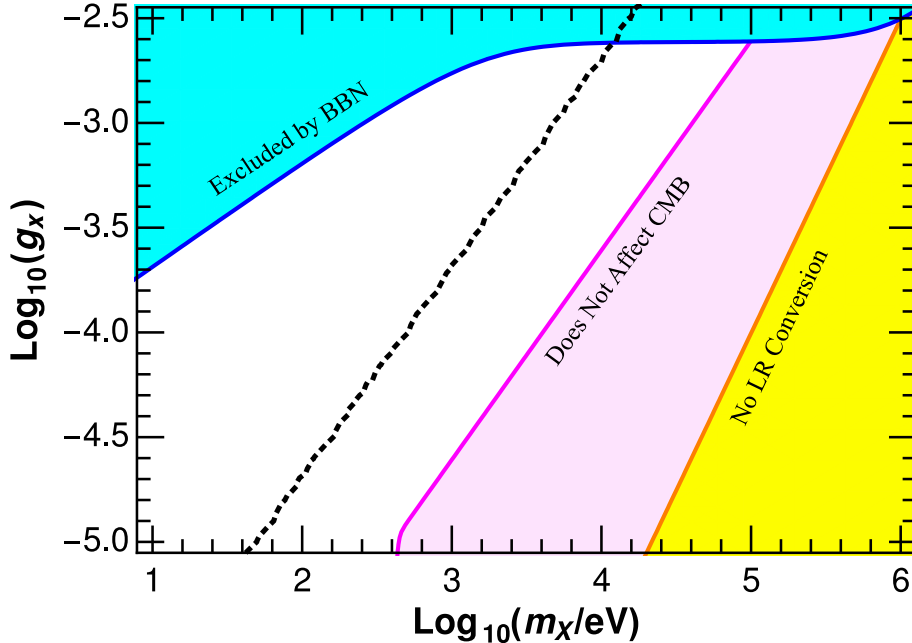


Figure 3: Constraints on the dark photon gauge coupling g_x and its mass m_X . Here we input a typical neutrino mass $m_\nu = 0.05$ eV. The blue region overproduces ν_R and X^μ before decoupling of the neutrino electroweak interaction and is therefore excluded by the BBN. In the yellow region, the conversion $\nu_L \rightarrow \nu_R, \nu_s$ is never efficient. In the pink region, neutrinos free-stream too early and behave effectively as the SM neutrinos for CMB observation. Only the white area is allowed. On the black dotted curve, right-handed neutrinos begin free-streaming at $z \sim 8000$, which is significantly delayed as compared to the standard Λ CDM model.

implies $n_R/2 = n_{\nu_R} = n_{\nu_s} = n_{\nu_L}$. This excludes the pink region in Fig. 3 for the typical neutrino mass value $m_\nu = 0.05$ eV (based on neutrino oscillation data). Finally, if the free-streaming of neutrinos starts too late, the neutrino self-scattering would strongly alter the low- ℓ part of the CMB power spectrum and thus deteriorate the fit to the observation [10]. We note that the recent studies of self-interacting-neutrino cosmology have a delayed onset of neutrino free-streaming at $z \sim 8000$ when modes of $\ell \approx 400$ enter the Hubble radius [9, 15]. We consider a similar onset time of free-streaming for the right-handed neutrinos in the current estimate. (A precise determination of the onset time of free-streaming needs a systematical fit of the CMB power spectrum which is beyond the current scope.) As a guideline, we consider the right-handed neutrinos to begin free-streaming at $z \sim 8000$, and plot this case in Fig. 3 as the black dotted curve.

Finally, we comment on the laboratory and astrophysical constraints. Our model conserves lepton number and is thus not constrained by the neutrinoless double-beta decay measurements [29, 30]. The major laboratory constraints on our model come from meson decays. The typical neutrino energy in these processes are $E_\nu \sim O(100\text{MeV}) > v_s$, so the chirality-flip factor of mass insertion $m_\nu/E_\nu \sim 10^{-9}$ is much smaller than the effective neutrino Yukawa coupling y' to the singlet Higgs boson σ , where $|y'| = O(10^{-7})$. This

means that the left-handed neutrinos ν_L from meson decays could emit dark photon X^μ only after the mass insertion with the suppression m_ν/E_ν , while ν_L can emit σ boson with the effective Yukawa coupling y' . Hence, we expect the effective Yukawa coupling y' to receive nontrivial constraint from meson decays via emitting σ bosons. The strongest constraint from meson decay on a scalar coupling to neutrinos [19] arises from measuring the light meson decay spectrum which was used to search for heavy neutrinos [20, 21]. This sets an upper bound $|y'|^2 < 3.8 \times 10^{-7}$. The neutrino emission of the Supernova 1987A [31, 32] may also be modified by the emission of σ bosons from the left-handed neutrinos trapped in the core³ through the vertex in Fig. 1a. From the result of [12], we derive an upper limit $|y'|^2 \lesssim (1-12) \times 10^{-5} / (1+m_\sigma/\text{keV})$. Both constraints are well satisfied since we have smaller Yukawa coupling $|y'| = O(10^{-7})$ in the current model.

In passing, we note that various non-zero ΔN_{eff} near the epoch of recombination may also help to reduce the Hubble tension to different levels. The right-handed neutrinos in our model are converted from left-handed neutrinos after their decoupling from the hot plasma of other SM particles and thus do not introduce ΔN_{eff} . The BBN constraint $\Delta N_{\text{eff}} \lesssim 0.5$ [17, 12] comes from the model-dependent baryon-to-photon ratio along with the measured primordial abundance of Y_p [33] and [D/H] [34]. To realize the model considered in Ref. [9] with $\Delta N_{\text{eff}} \approx 1$, the additional ΔN_{eff} needs to be generated in the epoch between BBN and recombination. This may be done by entropy injection from the dark sector [35]. Alternatively, one may assume a smaller ΔN_{eff} that is consistent with the BBN constraint at the expense of less reduction of Hubble tension as in the case of [11]. Due to the many possibilities of choosing ΔN_{eff} and its generation which is a rather model-dependent issue, our current study will focus on the realization of the neutrino self-interaction as an attractive major resolution.

In summary, we have demonstrated in this section that with a suitable choice of parameter space shown in Fig. 3, the left-handed neutrinos convert to the right-handed neutrinos only after the BBN. The final neutrino relic is a mixture of ν_L , ν_R and ν_s which scatter with each other before recombination. The evolution of the neutrino density is consistent with the BBN and our model is safe under the laboratory and supernovae constraints on hidden neutrino interactions.

4. Evolution of Neutrino Densities by Numerical Analysis

In this section, we will demonstrate the neutrino density evolution as discussed qualitatively in Section 3. For this, we solve the evolution of Boltzmann equation numerically for the $(\nu_L, \nu_R, \nu_s, X^\mu, \sigma)$ system with a given set of parameters. We first treat the particles

³The core-collapse process is not well understood, so the resultant bound should be considered as an estimate rather than a strict constraint [36].

$(\nu_R, \nu_s, X^\mu, \sigma)$ as a single tightly coupled fluid in the Boltzmann equation to avoid the numerical stiffness. Then, we present the numerical result and demonstrate that it is consistent with the physical picture given in Section 3.

In the parameter space of interest, the decay rate of X^μ and the scattering rate among σ, ν_s, ν_R and X^μ are dominated by the $U(1)_X$ gauge interaction and much larger than the Hubble rate as we have shown in Section 3. The system of Boltzmann equations that evolves the particle number densities $n_{\nu_L}, n_{\nu_R}, n_{\nu_s}, n_\sigma$ and n_X simultaneously is hard to solve numerically because of large hierarchies between scattering rates and the Hubble rate. To address this issue, we treat ν_s, ν_R, σ and X^μ as a single tightly coupled fluid \mathcal{T} with its number density parameterized by

$$n_{\mathcal{T}} = n_{\nu_R} + n_{\nu_s} + 2n_\sigma + 2n_X, \quad (4.1)$$

where n_{ν_R} and n_{ν_s} denote the total number densities including both particles and anti-particles summed over the three families. Since $\nu_R \bar{\nu}_s \leftrightarrow X^\mu$ and $\sigma \sigma \leftrightarrow X^\mu X^\mu$ dominate the conversion between species in \mathcal{T} , we see that under the definition of Eq.(4.1) the fast $U(1)_X$ processes do not change $n_{\mathcal{T}}$.⁴ The processes that evolve $n_{\mathcal{T}}$ or n_{ν_L} are those with at least a mass-insertion suppression in an external leg or with a Yukawa vertex of coupling y' such as those in Fig. 1a and Fig. 2. Thus, it is more convenient to solve just two Boltzmann equations for a system of n_{ν_L} and $n_{\mathcal{T}}$ instead, which does not involve the unsuppressed fast processes.

After each $n_{\mathcal{T}}$ changing interaction, the number density of each particle species in \mathcal{T} relaxes rapidly to a stationary configuration through $U(1)_X$ interaction. The distributions of $n_{\nu_R}, n_{\nu_s}, n_\sigma$ and n_X within $n_{\mathcal{T}}$ can be approximated by its stationary values governed by the detailed balance principle within the \mathcal{T} fluid. Then, the equilibrium of scattering processes $\nu_R \nu_R \leftrightarrow \nu_s \nu_s$ and $\sigma \sigma \leftrightarrow X^\mu X^\mu$ imposes:

$$\frac{n_{\nu_R}}{n_{\nu_s}} = \frac{n_{\nu_R}^{\text{eq}}}{n_{\nu_s}^{\text{eq}}} = 1, \quad \frac{n_{X^\mu}}{n_\sigma} = \frac{n_{X^\mu}^{\text{eq}}}{n_\sigma^{\text{eq}}} = 3. \quad (4.2)$$

Here n_j^{eq} is the equilibrium density of a particle in contact with a hot plasma,

$$n_j^{\text{eq}} = \frac{g_j}{(2\pi)^3} \int d^3p \frac{1}{\exp(E/T) \pm 1}, \quad (4.3)$$

with g_j being the degrees of freedom. Eq.(4.2) holds because n_j^{eq} also satisfies the detailed balance condition. Similarly, the equilibrium of the decay and inverse decay of $X^\mu \leftrightarrow \nu_R \bar{\nu}_s$ leads to the following conditions,

$$\frac{n_X^{\text{eq}}}{n_{\nu_s}^{\text{eq}} n_{\nu_R}^{\text{eq}}} = \frac{n_X}{n_{\nu_s} n_{\nu_R}} = \frac{n_X}{n_{\nu_s}^2}. \quad (4.4)$$

⁴The coefficient 2 of n_σ in Eq.(4.1) needs to be modified if one chooses to work with $m_\sigma > 2m_X$ instead. In this case, the process $\sigma \leftrightarrow X^\mu X^\mu$ is kinematically allowed.

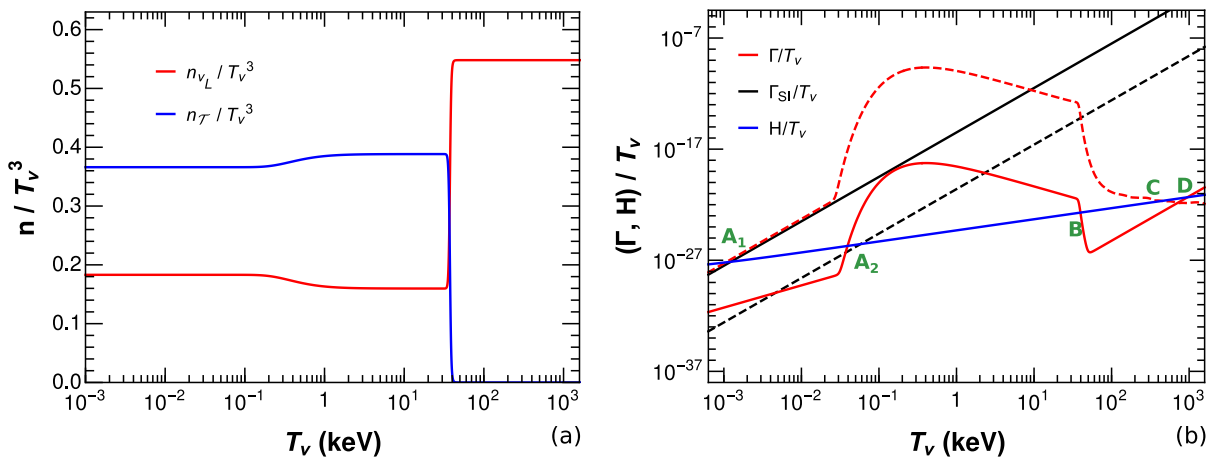


Figure 4: Panel (a): Evolutions of the scaled particle number densities of left-handed neutrinos n_{ν_L}/T_ν^3 (red curve) and tightly-coupled fluid $n_{\mathcal{T}}/T_\nu^3$ (blue curve) are shown as functions of T_ν (eV), for the interacting Dirac neutrino model with $m_\nu = 0.05$ eV, $v_s = 6$ MeV, and $m_X = 1$ keV. Panel (b): Scaled reaction rate Γ/T_ν and Hubble rate H/T_ν are plotted as functions of T_ν for our interacting Dirac neutrino model. The red solid (dashed) curve shows the interaction rate of left-handed (right-handed) Dirac neutrinos with $m_\nu = 0.05$ eV, $v_s = 6$ MeV, and $m_X = 1$ keV. The Hubble rate is shown in the blue curve. The black solid (dashed) curve shows the reaction rate of the strong (moderate) neutrino self-interaction with $G_{\text{eff}} = 10^{-1.35}(10^{-3.9}) \text{ MeV}^{-2}$, defined in Ref. [9]. Note that the vertical axis of panel (a) is plotted in linear scale, while it is in log-scale for panel (b).

With Eqs.(4.1)-(4.2) and (4.4), the number densities n_{ν_R} , n_{ν_s} , n_σ and n_X appearing in the reaction rates can be computed as a function of $n_{\mathcal{T}}$ and the temperature T . The Boltzmann equation and the expressions of thermally averaged cross sections and decay rates are presented in Appendix B. The fast reactions are contained within the \mathcal{T} fluid and do not appear in the equations as expected.

We solve the Boltzmann equations of the ν_L - \mathcal{T} system with the choice of parameters $m_\nu = 0.05$ eV, $v_s = 6$ MeV, and $m_X = m_\sigma = 1$ keV. Fig. 4 presents our results. In Fig. 4a, we plot the evolution of n_{ν_L}/T_ν^3 and $n_{\mathcal{T}}/T_\nu^3$ as a function of the neutrino temperature T_ν . The generation of the \mathcal{T} fluid becomes rather rapid at the temperature $T_\nu \approx 40$ keV, which is much later than the decoupling of neutrinos from other SM particles. This is the key feature of the cosmological evolution of our model as discussed in Section 3. When the temperature drops below ~ 100 eV in Fig. 4, X^μ and σ no longer remain in the \mathcal{T} fluid because of their large masses. The number densities of ν_L , ν_s and ν_R then equally share the initial total neutrino density $n_{\text{tot}} = n_{\nu_L} + n_{\nu_R} + n_{\nu_s}$, with $n_{\nu_L} = n_{\nu_s} = n_{\nu_R} = n_{\text{tot}}/3$.

In Fig. 4b, we plot the scaled reaction rate of neutrinos (Γ/T_ν) according to the evolution of densities in Fig. 4a. Here, the interaction rate of left-handed (right-handed) neutrinos is presented by the red solid (dashed) curve. The interaction rate of ν_s also follows the same red dashed curve as the right-handed neutrino ν_R . The Hubble rate is depicted by the blue curve. The intersections of the scattering rates and the Hubble rate

are distinctive epochs of the cosmological evolution, and we mark their locations by the bold letters **A**₁, **A**₂, **B**, **C**, and **D**, respectively. The scattering rate of the left-handed neutrino is initially dominated by the electroweak interaction at the very right side of the red solid curve. As the Universe cools down, the weak interaction becomes inefficient at the epoch **D** (the intersection of the red solid curve with the blue curve) and the neutrinos decouple from the hot plasma. In contrast, the reaction rate of the small amount of right-handed neutrinos for $T \gtrsim 40$ keV is dominated by its scattering with the left-handed neutrinos shown in Fig. 2. The reaction rate of the right-handed neutrinos (shown as the red dashed curve) intersects with the blue curve at epoch **C** slightly later than epoch **D**. The proximity of epochs **C** and **D** is a numerical coincidence and has no significance in the current analysis. The left-handed neutrinos begin to convert to right-handed ones through the processes shown in Fig. 2, but the conversion remains slow because n_{ν_R} and n_{ν_s} are extremely small at this epoch as shown in Fig. 4a. As the number densities n_{ν_R} and n_{ν_s} increase, the reaction rate of ν_L becomes dominated by its scattering with ν_R and ν_s , and the conversion becomes rapid at the epoch **B**. This corresponds to the sharp increase of $n_{\mathcal{T}}$ around $T=40$ keV in Fig. 4a. Note that the panels (a) and (b) in Fig. 4 are plotted in linear and log scale, respectively. Eventually, the neutrino gas becomes a mixture of ν_L , ν_s , and ν_R . The reaction rate of ν_R and ν_s gets dominated by the scattering between themselves such as the process in Fig. 1b. Because of the mass insertion, ν_L scatters less frequently than other components as is evident from the difference between the red dashed curve and the red solid curve. The left-handed neutrinos start to free-stream when $T \approx 40$ eV at the epoch **A**₂, much earlier than the right-handed neutrinos which start to free stream when $T \approx 1$ eV at the epoch **A**₁.

In comparison with the standard model (SM) neutrinos which start to free-stream at the epoch **D**, the delayed onset of neutrino free-streaming in our model leads to phase shifts and amplification of acoustic peaks in the CMB power spectrum; these effects may be compensated by the shifts of other cosmological parameters such as a larger Hubble constant. The previous study of the CMB power spectrum suggests [9] that a larger value of Hubble constant up to $H_0 = 72.3 \pm 1.4 \text{ km s}^{-1} \text{ Mpc}^{-1}$ can be accommodated for the CMB measurements with $\Delta N_{\text{eff}} \approx 1$ and slight adjustments of other cosmological parameters as long as the active neutrinos scatter with themselves through an effective interaction $G_{\text{eff}} \bar{\nu} \nu \bar{\nu} \nu$. This is a fairly model-independent approach since it does not depend on details of how this effective interaction arises. For this, Ref. [9] considered a “strongly interacting” scenario with $\log_{10}(G_{\text{eff}} \text{ MeV}^2) = -1.35_{-0.066}^{+0.12}$ and a “moderately interacting” scenario with $\log_{10}(G_{\text{eff}} \text{ MeV}^2) = -3.90_{-0.93}^{+1.0}$, which accommodate the Hubble constant of values $H_0 = 72.3 \pm 1.4 \text{ km s}^{-1} \text{ Mpc}^{-1}$ and $H_0 = 71.2 \pm 1.3 \text{ km s}^{-1} \text{ Mpc}^{-1}$, respectively. To make use of the fits of [9], in Fig. 4b we plot as a reference the reaction rate of the central value of the strong (moderate) neutrino self-interaction by the black solid

(dashed) curve. A direct numerical comparison of the reaction rate is given at the end of Appendix B. Despite some difference in the detailed form of the neutrino self-interactions, Fig. 4b shows that the right-handed (left-handed) neutrinos in our model start to free-stream at roughly the same epoch \mathbf{A}_1 (\mathbf{A}_2) as the reference scenario of the strongly (moderately) self-interacting neutrinos. So their impacts on the CMB power spectrum are mainly the same. Hence, the cosmic neutrino relic in our model can be regarded as a mixture of the two scenarios of strongly and moderately interacting neutrinos in Ref. [9]. Assuming entropy injection of $\Delta N_{\text{eff}} \simeq 1$ from the dark sector after the BBN as we discussed in Sections 3, the inferred Hubble constant from CMB observation of our model should lie between those of the strongly and moderately interacting regimes. Therefore, the late onset of neutrino free-streaming in our model is consistent with a larger Hubble constant of $H_0 \simeq (71 - 72) \text{ km s}^{-1} \text{ Mpc}^{-1}$ without deteriorating the fit to CMB observations. In this way, our model can mainly remove the tension with the local measurements of Hubble constant $H_0 = 74.0 \pm 1.4 \text{ km s}^{-1} \text{ Mpc}^{-1}$ [5].

A direct numerical comparison of the reaction rate with Ref. [9] is given at the end of our Appendix B. We find that with the choice of parameters $m_\nu = 0.05 \text{ eV}$ and $v_s = 6 \text{ MeV}$, the right-handed and left-handed neutrinos interact with the neutrino gas, which have effective 4-neutrino couplings $G_R = 10^{-1.24} \text{ MeV}^{-2}$ and $G_L = 10^{-4.38} \text{ MeV}^{-2}$, respectively, at $T \approx 10 \text{ eV}$. Hence, the right-handed neutrinos ν_R and ν_s (which make up 2/3 of the neutrino gas in our model) behave like the strongly self-interacting neutrinos of Ref. [9] with $\log_{10}(G_{\text{eff}} \text{ MeV}^2) = -1.35_{-0.066}^{+0.12}$, while the left-handed neutrinos ν_L (which make up the remaining 1/3 of the neutrino gas in our model) behave like the moderately self-interacting neutrinos with $\log_{10}(G_{\text{eff}} \text{ MeV}^2) = -3.90_{-0.93}^{+1.0}$ [9]. This is in accordance with our discussion of Fig. 4b.

The above numerical analysis demonstrates that the evolutions of both the number density and reaction rate are consistent with the physical picture of Section 3. Hence, we find that our current Dirac seesaw model provides a viable resolution to the Hubble tension problem, with wide parameter space shown in Fig. 3.

5. Conclusions

The discrepancy of the Hubble constant measurements concerns the cosmological observations inferred from the early and late Universe, and is fairly robust, ranging from 4σ to 6σ deviations [2]. If this tension persists, it would point to new physics in the dynamics of the cosmological expansion, beyond the standard Λ CDM cosmology. Such new physics resolution could arise from the exciting interface of particle physics and cosmology. In this work, we proposed a new realization of the self-interacting neutrino via Dirac seesaw to achieve the mechanism of shrinking down the physical size of sound horizon at the last

scattering surface, while keeping the projected Silk damping scale intact.

In Section 2, we presented a new Dirac seesaw model with an anomaly-free dark $U(1)_X$ gauge group, in which the light dark photon serves as the mediator and couples only to the right-handed components of Dirac neutrinos. It naturally generates small masses for Dirac neutrinos and induces effective self-interaction for the right-handed neutrinos. We made no assumption of the flavor structure for neutrino self-interactions, unlike the models in the previous literature [12]. Our model can evade both the cosmological and laboratory constraints because the coupling between the left-handed neutrinos and the dark photon mediator is extremely weak in high energy processes due to the chirality-flip suppression factor m_ν/E_ν (Fig. 2).

In Sections 3 and 4, we studied the cosmological evolution of the left/right-handed neutrinos, which has nontrivial behaviour because of the gauge interactions mediated by dark photon. We first presented the estimates in Section 3, and the constraints on the dark photon parameter space in Fig. 3. We then performed numerical analysis of evolving Boltzmann equations of neutrino densities in Section 4. We demonstrated that after the neutrino decoupling and for a proper choice of the mediator mass and coupling, part of the left-handed neutrinos converts into right-handed particles ν_R and ν_s in a very short epoch between the BBN and recombination. The conversion occurs much later than the neutrino decoupling from the hot plasma of other SM particles, so it does not generate extra ΔN_{eff} which would violate the BBN bound. The right-handed particles are more reactive and couple tightly to the left-handed neutrinos. The resultant non-free-streaming neutrinos ν_L , ν_R and ν_s cause phase shifts and amplification of acoustic peaks in the CMB power spectrum, which is a key ingredient of the resolution to the Hubble tension. Our findings are presented in Fig. 4. Setting entropy injection of $\Delta N_{\text{eff}} \simeq 1$ after the BBN, we found that the late onset of neutrino free-streaming in our model is consistent with a larger Hubble constant up to $H_0 \simeq (71-72) \text{ km s}^{-1} \text{ Mpc}^{-1}$ without deteriorating the fit to CMB data [9]. This reduces the H_0 discrepancy down to 1σ level and thus mainly resolves the Hubble tension by our new scenario of self-interacting neutrinos.

Finally, we note that the left-handed neutrinos and right-handed neutrinos scatter at different rates in the early Universe and it provides an interesting target for the analysis of self-interacting neutrino cosmology. The hidden $U(1)_X$ interaction is currently unconstrained by laboratory experiments, but on the other hand it signifies the role of the CMB observation to probe non-standard neutrino interactions. The hidden neutrino interaction may leave a trace on the cosmic neutrino background where the neutrino energy is extremely small and the chirality-flip factor is no longer a suppression.

Acknowledgments

JZ thanks Shaofeng Ge for an early discussion. HJH and JZ were supported in part by NSF of China (No.11675086 and 11835005), and also by CAS Center for Excellence in Particle Physics (CCEPP), National Key R&D Program of China (No.2017YFA0402204), Shanghai Laboratory for Particle Physics & Cosmology (No.11DZ2260700), and Office of Science & Technology, Shanghai Municipal Government (No.16DZ2260200). YZM acknowledges the support of NRF-120385, NRF-120378, and NSFC-11828301.

A. Neutrino Chirality Flip via Mass-Insertion

In this appendix, we re-derive the chirality-flip factor via mass-insertion for clarity and completeness. For each insertion of neutrino mass, an external line of the left-handed neutrino in the Feynman diagram is modified as

$$\chi_-(p) \rightarrow \frac{m_\nu p_\mu \bar{\sigma}^\mu}{p^2} \chi_-(p), \quad (\text{A.1})$$

where χ_- is the left-handed 2-component spinor eigenfunction. For simplicity, we choose the reference frame such that the direction of the neutrino momentum \vec{p} is along $+\hat{z}$, and $\chi_-(p) = \sqrt{p^0 + p^3} \begin{pmatrix} 0 \\ 1 \end{pmatrix}$. In the limit of $p^0 \rightarrow p^3$, the pole factor $(p^0 - p^3)$ in the denominator will be cancelled by that in the numerator, and thus we have

$$\frac{m_\nu p_\mu \bar{\sigma}^\mu}{p^2} \begin{pmatrix} 0 \\ 1 \end{pmatrix} \rightarrow \frac{m_\nu}{2p^0} \begin{pmatrix} 0 \\ 1 \end{pmatrix}. \quad (\text{A.2})$$

This result is also evident from the massive 4-component Dirac spinor: the right-handed component of a spin-down fermion moving along $+\hat{z}$ contains a factor $m_\nu/(2p^0)$ in the leading order of m_ν . So each mass-insertion in the external line leads to a factor m_ν/\sqrt{s} in the amplitude.

B. Boltzmann Equations and Cross Sections

In this appendix, we give the relevant Boltzmann equations used to evolve the number density in Fig.4. As we described in Section 4, we treat σ , ν_s , ν_R and X^μ as a single fluid \mathcal{T} characterized by the number density $n_{\mathcal{T}} = n_{\nu_R} + n_{\nu_s} + 2n_\sigma + 2n_X$. The number density of each component of \mathcal{T} relaxes rapidly to its stationary distribution after the scattering with ν_L . So we can approximate their number density as a function of $n_{\mathcal{T}}$ and temperature T_ν given by the solution of Eqs.(4.1)-(4.2) and Eq.(4.4).

The Boltzmann equations which govern the evolution of n_{ν_L} and $n_{\mathcal{T}}$ are given by

$$\begin{aligned} \frac{dn_{\nu_L}}{dt} + 3Hn_{\nu_L} &= -n_{\nu_L}n_R\langle\sigma v\rangle_{LR\sigma} - n_{\nu_L}n_R\langle\sigma v\rangle_{LRX} - n_{\nu_L}n_R\langle\sigma v\rangle_{LR} \\ &\quad + \frac{1}{2}n_R^2\langle\sigma v\rangle_{LR} + n_X\Gamma_{XLR} + n_\sigma\Gamma_\sigma, \end{aligned} \quad (\text{B.1a})$$

$$\begin{aligned} \frac{dn_{\mathcal{T}}}{dt} + n_{\mathcal{T}} &= -\frac{1}{2}n_R^2\langle\sigma v\rangle_{LR} - n_X\Gamma_{XLR} - n_\sigma\Gamma_\sigma \\ &\quad + n_{\nu_L}n_R\langle\sigma v\rangle_{LR\sigma} + n_{\nu_L}n_R\langle\sigma v\rangle_{LRX} + n_{\nu_L}n_R\langle\sigma v\rangle_{LR} \\ &\quad + n_{\nu_L}^2\left(\frac{m_\nu}{m_\sigma}\right)^2\langle\sigma v\rangle_{LR\sigma}, \end{aligned} \quad (\text{B.1b})$$

where $n_R \equiv n_{\nu_R} + n_{\nu_s} = 2n_{\nu_R}$. (Here we recall that in our notation, each number density n_j contains both the particles and anti-particles from all families.) For completeness, we also provide the thermally averaged cross sections used in the Boltzmann equation.⁵ We compute the thermally averaged decay rates as follows,

$$\Gamma_{XLR} = \frac{3m_\nu^2 m_X}{8v_s^2 \pi} \frac{K_1(m_X/T)}{K_2(m_X/T)}, \quad (\text{B.2a})$$

$$\Gamma_\sigma = \frac{3m_\nu^2 m_\sigma}{8v_s^2 \pi} \frac{K_1(m_\sigma/T)}{K_2(m_\sigma/T)}, \quad (\text{B.2b})$$

$$\Gamma_X = \frac{m_X^3}{4v_s^2 \pi} \frac{K_1(m_X/T)}{K_2(m_X/T)}. \quad (\text{B.2c})$$

Γ_X and Γ_σ are the thermally averaged decay rate of X^μ and σ , respectively. Γ_{XLR} is the partial decay rate of X^μ to $\nu_L \bar{\nu}_s$, $\nu_s \bar{\nu}_L$. Note that for simplicity we have set $m_\sigma = m_X$ and thus the decay mode $\sigma \rightarrow X^\mu X^\mu$ is forbidden.

The thermally averaged inverse decay rates are obtained from the decay rates by the principle of detailed balance,

$$\langle\sigma v\rangle_{RRX} = \frac{2n_X^{\text{eq}}}{n_R^2} \Gamma_X, \quad (\text{B.3a})$$

$$\langle\sigma v\rangle_{LRX} = \frac{n_\sigma^{\text{eq}}}{n_R^{\text{eq}} n_{\nu_L}^{\text{eq}}} \Gamma_{XLR}, \quad (\text{B.3b})$$

$$\langle\sigma v\rangle_{LR\sigma} = \frac{n_\sigma^{\text{eq}}}{n_R^{\text{eq}} n_{\nu_L}^{\text{eq}}} \Gamma_\sigma, \quad (\text{B.3c})$$

where $\langle\sigma v\rangle_{RRX}$, $\langle\sigma v\rangle_{LRX}$ and $\langle\sigma v\rangle_{LR\sigma}$ are the thermally averaged cross sections of $\nu_R R \rightarrow X^\mu$, $\nu_L R \rightarrow X^\mu$ and $\nu_L R \rightarrow X^\mu$, respectively. Here R denotes any particle from any family of ν_R , ν_s or their antiparticles. The cross section computed is the average over all possible choices of R . The number density n_j^{eq} is the equilibrium density of a given type of particles in contact with a thermal bath,

$$n_j^{\text{eq}} \equiv \frac{g_j}{(2\pi)^3} \int \frac{d^3p}{\exp(E/T) \pm 1}, \quad (\text{B.4})$$

⁵For instance, see Refs. [37, 38] for the method of computing thermally averaged cross sections.

with g_j the corresponding degrees of freedom.

Finally, the thermally averaged cross sections for the $2 \rightarrow 2$ scattering processes are

$$\langle \sigma v \rangle_{RR} = \begin{cases} \frac{35T^2}{6\pi v_s^4}, & (T \ll m_X), \\ \frac{m_X^2}{4\pi v_s^4}, & (T \gg m_X), \end{cases} \quad (\text{B.5a})$$

$$\langle \sigma v \rangle_{LR} = \begin{cases} \frac{35m_\nu^2}{144\pi v_s^4}, & (T \ll m_X), \\ \frac{m_\nu^2 m_X^2}{32\pi v_s^4 T^2}, & (T \gg m_X), \end{cases} \quad (\text{B.5b})$$

where $\langle \sigma v \rangle_{LR}$ and $\langle \sigma v \rangle_{RR}$ are the thermally averaged cross sections of processes $\nu_L R \rightarrow RR$ and $\nu_R R \rightarrow RR$, respectively. Again, we have averaged over all possible choices of R from any family of ν_R and ν_s , or their antiparticles. For simplicity, we neglect the masses in the propagators and approximate the cross sections as piece-wise functions of their limits of $T \ll m_X$ and $T \gg m_X$. This leads to the discontinuity for the slope of the red curve in Fig. 4a.

For comparison, we also compute the thermally averaged cross section of the neutrino self-interaction in Ref. [9]. In this fairly model-independent approach, the active neutrino interaction is parameterized by the squared amplitude,⁶

$$|\mathcal{M}|_{\nu_i}^2 \equiv \sum_{\text{spin}} \sum_{j,k,l} |\mathcal{M}|_{\nu_i + \nu_j \rightarrow \nu_k + \nu_l}^2 = 2G_{\text{eff}}^2 (s^2 + t^2 + u^2). \quad (\text{B.6})$$

This leads to a thermally averaged cross section,

$$\frac{1}{4} \sum_{\text{spin}} \langle \sigma v \rangle_{\text{SI}} = \frac{11}{4\pi} G_{\text{eff}}^2 T^2. \quad (\text{B.7})$$

Then, we can compare directly the scattering rate Γ_{SI} of the neutrino self-interaction in Ref. [9] to the rates of the right-handed neutrinos Γ_R and the left-handed neutrinos Γ_L in our model for $T \ll m_X$,

$$\frac{\Gamma_{\text{SI}}}{\Gamma_R} = \frac{\frac{1}{4} \sum_{\text{spin}} \langle \sigma v \rangle_{\text{SI}} n_{\nu_j}}{\langle \sigma v \rangle_{RR} (n_{\nu_R} + n_{\nu_s})} = \frac{G_{\text{eff}}^2}{G_R^2}, \quad (\text{B.8a})$$

$$\frac{\Gamma_{\text{SI}}}{\Gamma_L} = \frac{\frac{1}{4} \sum_{\text{spin}} \langle \sigma v \rangle_{\text{SI}} n_{\nu_j}}{\langle \sigma v \rangle_{LR} (n_{\nu_R} + n_{\nu_s})} = \frac{G_{\text{eff}}^2}{G_L^2}. \quad (\text{B.8b})$$

⁶We thank Francis-Yan Cyr-Racine for explaining the convention of Ref. [9] via email correspondence.

Here we have defined the effective coupling constants G_L and G_R for direct comparison with the G_{eff} in (B.6) from Ref. [9],

$$G_R = \sqrt{\frac{140}{33}} \frac{1}{v_s^2}, \quad (\text{B.9a})$$

$$G_L = \sqrt{\frac{35}{198}} \frac{m_\nu}{T} \frac{1}{v_s^2}. \quad (\text{B.9b})$$

Note that in our model ν_R and ν_s make up $2/3$ of the neutrino relics. So we have $n_{\nu_R} + n_{\nu_s} = (2/3)n_{\text{tot}}$ with n_{tot} the total relic neutrino density. Ref. [9] considered the scattering between Majorana neutrinos and $n_{\nu_j} = n_{\text{tot}}/3$ is the neutrino number density for each flavor. For $m_\nu = 0.05 \text{ eV}$ and $v_s = 6 \text{ MeV}$ as we choose in Sec.4, we obtain $G_R = 10^{-1.24} \text{ MeV}^{-2}$ and $G_L = 10^{-4.38} \text{ MeV}^{-2}$ at $T \approx 10 \text{ eV}$. Hence, the right-handed and left-handed neutrinos in our model behave like the strongly and moderately self-interacting neutrinos of Ref. [9] with the effective coupling $\log_{10}(G_{\text{eff}} \text{ MeV}^2) = -1.35_{-0.066}^{+0.12}$ and $\log_{10}(G_{\text{eff}} \text{ MeV}^2) = -3.90_{-0.93}^{+1.0}$, respectively.

References

- [1] J. L. Bernal, L. Verde, and A. G. Riess, “The trouble with H_0 ”, JCAP 1610 (2016) 019 [arXiv:1607.05617 [astro-ph.CO]].
- [2] L. Verde, T. Treu, and A. G. Riess, “Tensions between the Early and the Late Universe”, Nature Astronomy 3 (2019) 891 [arXiv:1907.10625 [astro-ph.CO]].
- [3] N. Aghanim *et al.* [Planck Collaboration], “Planck 2018 Results. VI. Cosmological Parameters”, arXiv:1807.06209 [astro-ph.CO].
- [4] T. M. C. Abbott *et al.* [DES Collaboration], “Dark Energy Survey Year 1 Results: A Precise H_0 Estimate from DES Y1, BAO, and D/H Data”, Mon. Not. Roy. Astron. Soc. 480 (2018) 3879, no. 3 [arXiv:1711.00403 [astro-ph.CO]].
- [5] A. G. Riess, S. Casertano, W. Yuan, L. M. Macri, and D. Scolnic, “Large Magellanic Cloud Cepheid Standards Provide a 1% Foundation for the Determination of the Hubble Constant and Stronger Evidence for Physics beyond Λ CDM”, Astrophys. J. 876 (2019) 85, no. 1 [arXiv:1903.07603 [astro-ph.CO]].
- [6] M. Rameez and S. Sarkar, “Is There Really a ‘Hubble Tension?’”, arXiv:1911.06456 [astro-ph.CO].
- [7] K. C. Wong *et al.*, “H0LiCOW XIII. A 2.4% Measurement of H_0 from Lensed Quasars: 5.3σ Tension between Early and Late-Universe Probes”, arXiv:1907.04869 [astro-ph.CO].

- [8] F. Y. Cyr-Racine and K. Sigurdson, “Limits on neutrino-neutrino scattering in the early universe”, *Phys. Rev. D* 90 (2014) 123533, no. 12 [arXiv:1306.1536 [astro-ph.CO]].
- [9] C. D. Kreisch, F. Y. Cyr-Racine, and O. Dore, “The neutrino puzzle: anomalies, interactions, and cosmological tensions”, arXiv:1902.00534 [astro-ph.CO].
- [10] F. Forastieri, M. Lattanzi and P. Natoli, “Cosmological constraints on neutrino self-interactions with a light mediator”, *Phys. Rev. D* 100 (2019) 103526, no. 10, [arXiv:1904.07810 [astro-ph.CO]].
- [11] S. Ghosh, R. Khatri, and T. S. Roy, “Dark Neutrino interactions phase out the Hubble tension”, arXiv:1908.09843 [hep-ph].
- [12] N. Blinov, K. J. Kelly, G. Z. Krnjaic, and S. D. McDermott, “Constraining the Self-Interacting Neutrino Interpretation of the Hubble Tension”, *Phys. Rev. Lett.* 123 (2019) 191102, no. 19 [arXiv:1905.02727 [astro-ph.CO]].
- [13] N. Blinov and G. Marques-Tavares, arXiv:2003.08387 [astro-ph.CO].
- [14] I. M. Oldengott, T. Tram, C. Rampf, and Y. Y. Y. Wong, “Interacting neutrinos in cosmology: exact description and constraints,” *JCAP* 1711 (2017) 027 [arXiv:1706.02123 [astro-ph.CO]].
- [15] L. Lancaster, F. Y. Cyr-Racine, L. Knox, and Z. Pan, “A tale of two modes: neutrino free-streaming in the early universe”, *JCAP* 1707 (2017) 033 [arXiv:1704.06657 [astro-ph.CO]].
- [16] R. H. Cyburt, B. D. Fields, K. A. Olive, and T. H. Yeh, “Big Bang Nucleosynthesis: 2015”, *Rev. Mod. Phys.* 88 (2016) 015004 [arXiv:1505.01076 [astro-ph.CO]].
- [17] A. Berlin, N. Blinov, and S. W. Li, “Dark Sector Equilibration During Nucleosynthesis”, *Phys. Rev. D* 100 (2019) 015038, no. 1 [arXiv:1904.04256 [hep-ph]].
- [18] E. Grohs, G. M. Fuller, and M. Sen, “Consequences of neutrino self interactions for weak decoupling and big bang nucleosynthesis”, arXiv:2002.08557 [astro-ph.CO].
- [19] P. S. Pasquini and O. L. G. Peres, “Bounds on Neutrino-Scalar Yukawa Coupling”, *Phys. Rev. D* 93 (2016) 053007, no. 5; Erratum: *Phys. Rev. D* 93 (2016) 079902, no. 7, [arXiv:1511.01811 [hep-ph]].
- [20] D. I. Britton *et al.*, “Improved search for massive neutrinos in $\pi^+ \rightarrow e^+$ neutrino decay”, *Phys. Rev. D* 46 (1992) R885.

- [21] A. V. Artamonov *et al.* [E949 Collaboration], “Search for heavy neutrinos in $K^+ \rightarrow \mu^+ \nu_H$ decays”, Phys. Rev. D 91 (2015) 052001, no. 5; Erratum: Phys. Rev. D 91 (2015) 059903, no. 5, [arXiv:1411.3963 [hep-ex]].
- [22] J. G. Rodrigues, M. Benetti, M. Campista, and J. Alcaniz, “Probing the Seesaw Mechanism with Cosmological data”, arXiv:2002.05154 [astro-ph.CO].
- [23] M. Escudero and S. J. Witte, “A CMB Search for the Neutrino Mass Mechanism and its Relation to the H_0 Tension”, arXiv:1909.04044 [astro-ph.CO].
- [24] J. Sakstein and M. Trodden, “Early dark energy from massive neutrinos – a natural resolution of the Hubble tension”, arXiv:1911.11760 [astro-ph.CO].
- [25] J. Gehrlein and M. Pierre, “A testable hidden-sector model for Dark Matter and neutrino masses”, JHEP 2002 (2020) 068 [arXiv:1912.06661 [hep-ph]].
- [26] P.-H. Gu and H.-J. He, “Neutrino Mass and Baryon Asymmetry from Dirac Seesaw”, JCAP 0612 (2006) 010 [arXiv:hep-ph/0610275].
- [27] M. Tanabashi *et al.*, [Particle Data Group], Phys. Rev. D 98 (2018) 030001.
- [28] J. Jaeckel, “A force beyond the Standard Model – Status of the quest for hidden photons”, Frascati Phys. Ser. 56 (2012) 172 [arXiv:1303.1821 [hep-ph]].
- [29] M. Agostini *et al.*, “Results on $\beta\beta$ decay with emission of two neutrinos or Majorons in ^{76}Ge from GERDA Phase I”, Eur. Phys. J. C 75 (2015) 416, no. 9 [arXiv:1501.02345 [nucl-ex]].
- [30] K. Blum, Y. Nir and M. Shavit, “Neutrinoless double-beta decay with massive scalar emission”, Phys. Lett. B 785 (2018) 354 [arXiv:1802.08019 [hep-ph]].
- [31] K. Hirata *et al.* [Kamiokande-II Collaboration], “Observation of a Neutrino Burst from the Supernova SN1987a”, Phys. Rev. Lett. 58 (1987) 1490
- [32] R. M. Bionta *et al.*, “Observation of a Neutrino Burst in Coincidence with Supernova SN1987a in the Large Magellanic Cloud”, Phys. Rev. Lett. 58 (1987) 1494.
- [33] E. Aver, K. A. Olive and E. D. Skillman, “The effects of He I $\lambda 10830$ on helium abundance determinations”, JCAP 1507 (2015) 011 [arXiv:1503.08146 [astro-ph.CO]].
- [34] R. J. Cooke, M. Pettini and C. C. Steidel, “One Percent Determination of the Primordial Deuterium Abundance”, Astrophys. J. 855 (2018) 102, no. 2 [arXiv:1710.11129 [astro-ph.CO]].

- [35] J. Alcaniz, N. Bernal, A. Masiero and F. S. Queiroz, “Light Dark Matter: A Common Solution to the Lithium and H_0 Problems”, arXiv:1912.05563 [astro-ph.CO].
- [36] N. Bar, K. Blum, and G. D’amico, “Is there a supernova bound on axions?” arXiv:1907.05020 [hep-ph].
- [37] P. Gondolo and G. Gelmini, “Cosmic abundances of stable particles: Improved analysis”, Nucl. Phys. B 360 (1991) 145.
- [38] M. Srednicki, R. Watkins, and K. A. Olive, “Calculations of Relic Densities in the Early Universe”, Nucl. Phys. B 310 (1988) 693.